Interannual variability of the North Atlantic Ocean sea level anomalies from Altimeter Observations

Athina Karaoli
4890523

Foteini Stavropoulou
9285520

Anna de Vries
7585047

Utrecht University

October 2021

Abstract

In this study we investigate the North Atlantic Ocean Circulation using sea level anomaly altimeter observations. From Empirical Orthogonal Function (EOF) decomposition we find the first mode representing around 6% of the data. The EOF1 illustrates the characteristic dipole pattern of this region with positive sea level anomalies in the suptropical gyre and negative sea level anomalies in the supbolar gyre. Following Kaiser's rule we use the first 86 EOF's that explain around 78% of the variance, to reconstruct the data. Furthermore, from correlation analysis we find highest positive correlation between our data and the annual Florida current (r = 0.88), and our data and the North Atlantic Oscillation in winter (r = 0.71). We find the two highest negative correlations between our data and the annual Atlantic Meridional Mode (r = -0.76), and our data and the annual Tropical North Atlantic index (r = -0.68).

1 Introduction

The ocean circulation in the North Atlantic is an important component in the heat and freshwater budget, with profound regional and global climate impacts. It consists of two gyres, the anti-clockwise North Altantic Subpolar Gyre and the clockwise North Atlantic (Subtropical) Gyre. The North Atlantic Gyre is subdivided into four inter-connected currents: the Gulf Stream of the west, the North Atlantic Current (or North Atlantic Drift) across the north, the Canary Current flowing southward along the east, and the Atlantic's North Equatorial Current in the south. Both gyres are important components of the global thermohaline circulation [1].

In this project, the variations of the sea level over the North Atlantic ocean are studied. Fig. 1 illustrates the Sea Level Anomalies (SLA) which were recorded in May 2020. Along the North Atlantic Ocean, the water level height fluctuates with an absolute maximum amplitude 0.15m. These sea level fluctuations are associated with the water's temperature, its salinity, the pressure of the atmosphere above the ocean surface and ocean currents [2].

In Fig. 2 the standard deviation of monthly mean SLA in North Atlantic is visualised. We clearly see that the highest standard deviation, with a value of 0.15, is to be found a few degrees from the coast of North-America and extends till 40°W and between 35°N and 50°N. This is partly where the Gulf Stream and North Atlantic Drift are located [1]. In addition, high standard deviations can be seen in the region crossing the

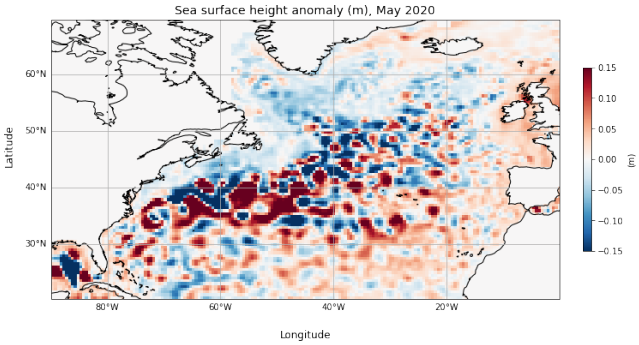

Fig. 1. North Atlantic sea level anomalies in [m] from altimeter observations for May 2020.

Atlantic Ocean towards Spain which also corresponds to the location of the Atlantic Drift. In the left low corner (90 − 80°W) we find another region with high standard deviations where the Florida Current is located.

The aim of the present study is to investigate the interannual variability of the North Atlantic Ocean Circulation based on sea level anomaly altimetry observations and examine the sensitivity of these variations to the large-scale atmosphere variability.

The paper is organized as follows: section 2 describes the satellite data set and the climate indices used in this study, section 3 includes detailed information about the methods used to analyse the data such as the Empirical Orthogonal Analysis (EOF) and the correlation analysis, section 4 describes the results

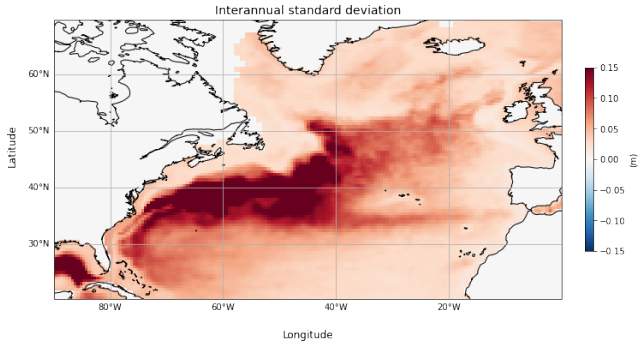

Fig. 2. Standard deviation of of the interannual sea level anomalies in [m] from altimeter observations.

of both of the two analysis that we used with all the relevant figures, and section 5 closes the paper with discussion and conclusions.

2 Data

The study of the interannual variability of the North Atlantic Ocean Circulation is based on SLA observations from a series of altimetry satellites. In general, satellite altimetry measures the sea surface topography and its change in time by using radar pulses. Because the sea surface height is in constant movement, it can be calculated only relative to Earth's surface. The Earth's surface is known as reference ellipsoid due to the Earth's ellipsoidal shape. The satellite is located in a certain altitude H from the theoretical reference ellipsoid. The satellite altimetry measures the vertical distance between the satellite and the sea surface through measuring the time it takes for a radar pulse to travel from the satellite to the surface and backwards. This distance is known as the satellite-to-surface range R. Thus, the difference between the satellite's position with respect to the reference ellipsoid H, and the satellite-to-surface range R corresponds to the sea level anomaly [3][4].

The satellite altimetry data is downloaded from the Copernicus Marine Service. The data contains monthly sea surface height anomalies (1993-2020) with respect to a 20-year mean reference period (1993-2012). These measurements are estimated by Optimal Interpolation, merging the measurement from different altimeter missions. This product is processed by the Data Unification and Altimeter Combination System (DUACS), a multimission altimeter data processing system. It processes data from all altimeter missions: Jason-3, Sentinel-3A, HY-2A, Saral/AltiKa, Cryosat-2, Jason-2, Jason-1, T/P, ENVISAT, GFO, ERS1/2.

The long-term trend and the seasonal cycle were already removed from the data. This was done because, as we investigate the interannual variability of the data set, both components would give the dominant signal in the time series represented by the two first Empirical orthogonal functions (EOF) modes [5].

The spatial resolution of the data is 0.25×0.25 but it is regridded to 0.5×0.5 to reduce the file size. The data covers the Atlantic region between 20.25°N-69.75°N and 90°W-0°E, for the period April 1993 to May 2020 at a monthly resolution, and units are 'meter' (with respect to the long-term sea level height).

Moreover, climate indices were used for correlation analysis as a further study for the main mode of variability. The climate indices used are: the North Atlantic Oscillation (NOA), the Greenland Blocking Index (GBI), the Atlantic Multidecadal Oscillation (AMO), the Arctic Oscillation (AO), the Tropical Northern Atlantic Index (TNA), the Atlantic Meridional Mode (AMM), the El Niño-Southern Oscillation (ENSO) and the Florida Current (FC). The data of the FC is downloaded from the KNMI's Climate Explorer while the other datasets are downloaded from the NOAA Physical Sciences Laboratory. The NAO index is based on the surface sea-level pressure difference between 20°N-90°N, for the period to 1950-2020. The GBI represents the mean 500 hPa geopotential height for the 60-80°N, 20-80°W region. It measures blocking (i.e., high-pressure systems that stay in place for an extended time) over Greenland for the period 1850-2020. The AMO index represents area-weighted average sea surface temperatures over the North Atlantic over the period 1870-2020. The AO index is constructed by projecting the 1000mb geopotential height anomalies from latitudes 20°N to 90°N over the period 1950-2021. The TNA index represents sea-surface temperatures from 5.5°N to 23.5°N and 15°W to 57.5°W over the period 1948-2021. The AMM index is defined as the leading mode of non-ENSO coupled ocean - atmosphere variability in the Atlantic basin [6]. The AMM spatial pattern is defined via applying Maximum Covariance Analysis (MCA) to Sea Surface Temperature (SST) and the zonal and meridional components of the 10m wind field [7] over the time period 1948-2021 over ocean regions between 21°S-32°N, 74°W-15°E. The Niño regions represent averaged sea temperature anomalies in ocean regions affected by El Niño and La Niña events. Four regions are considered: NINO12 (0-10°S, 80-90°W), NINO3 (5°S-5°N; 150°W-90°W), NINO34 (5°S-5°N; 170°W-120°W) and NINO4 (5°S-5°N: 160°E-150°W). The time span for the above El Niño data is between 1870-2020. Finally, the FC index is based on volumetric flow rate over eastern coast of Florida over the period 1982-2021. The FC data includes missing values, therefore for the correlation analysis, the period 2008-2012 is used where the data is complete. All the indices are provided as monthly time series.

3 Methods

In this exercise we use the Empirical Orthogonal Functions (EOF) decomposition method or otherwise known as Principle Component Analysis (PCA), which is a dimensionality-reduction method that is used to reduce the dimensionality of large data sets, by trans-

forming a large set of variables into a smaller one that still contains most of the information as the large set does [8]. The EOF method decomposes the data set into orthogonal basis functions by minimizing the distance between the orthogonal basis and the data [9]. Every function or mode explains part of the signal with the first mode explaining most of the signal and the second representing the remaining most of the signal, etc. We use the EOF method to identify the most important modes describing the data set.

To find these modes we firstly need to arrange the data into a matrix $X_{m,n}$ (1) with m vectors containing the variables we are interested in (the sea level anomaly at time m in our case) measured at n locations. Therefore, we create a $2-D$ matrix with the rows corresponding to time and columns to our spatial data points or position by reshaping our initial data set.

$$X_{m,n} = \begin{pmatrix} x_{1,1} & x_{1,2} & \cdots & x_{1,n} \\ x_{2,1} & x_{2,2} & \cdots & x_{2,n} \\ \vdots & \vdots & \ddots & \vdots \\ x_{m,1} & x_{m,2} & \cdots & x_{m,n} \end{pmatrix} \tag{1}$$

Next, we centre the data by subtracting the column mean from each column of matrix (1) and creating matrix (2).

$$X_c = \begin{pmatrix} x_{1,1} - \bar{x}_1 & x_{1,2} - \bar{x}_2 & \cdots & x_{1,n} - \bar{x}_n \\ x_{2,1} - \bar{x}_1 & x_{2,2} - \bar{x}_2 & \cdots & x_{2,n} - \bar{x}_n \\ \vdots & \vdots & \ddots & \vdots \\ x_{m,1} - \bar{x}_1 & x_{m,2} - \bar{x}_2 & \cdots & x_{m,n} - \bar{x}_n \end{pmatrix} \tag{2}$$

where $\bar{x}_i$, with $i = 1, 2, ..., n$, is the mean of the i_{th} variable.

Afterwards, we calculate the variance-covariance matrix as visualised in eq. (3).

$$C = \frac{1}{m-1} {X_c}^T X_c = \begin{pmatrix} \sigma_1^2 & \sigma_{1,2} & \cdots & \sigma_{1,n} \\ \sigma_{2,1} & \sigma_2^2 & \cdots & \sigma_{2,n} \\ \vdots & \vdots & \ddots & \vdots \\ \sigma_{m,1} & \sigma_{m,2} & \cdots & \sigma_n^2 \end{pmatrix} \tag{3}$$

where X_c^T denotes the transpose of X_c, σ_i^2, with $i = 1, 2, ..., n$, is the variance of the i_{th} variable and $\sigma_{j,i}^2$, with $j = 1, 2, ..., m$, is the covariance between the j_{th} and i_{th} variables.

The EOF method looks for patterns in the data that explain most of the variance by looking at the covariance or correlations between the variables. By solving eq. (4), we can determine the eigenvalues of $\mathbf{C}$.

$$det(\mathbf{C} - \lambda \cdot \mathbf{I}) = 0 \tag{4}$$

where $\mathbf{I}$ is the identity matrix.

The covariance matrix and the eigenvalues can now be combined in eq. (5).

$$C \cdot e_i = \lambda_i \cdot e_i \tag{5}$$

where λ_i is the eigenvalue and e_i is the eigenvector of size $\mathrm{n}\times 1$. The eigenvector points into the direction in which the data is stretched by the transformation to compute covariance while the eigenvalue is the factor by which the eigenvector is stretched or scaled to explain the variance [10][11]. The eigenvectors represent an alternative orthonormal coordinate system that describes the data set we are working with [9]. Each eigenvector has a corresponding "Principle Component" (time series) which explains variance in the time dimension. The pair of eigenvector and principle component define a mode that explains variance.

By ranking our eigenvectors in order of their eigenvalues, highest to lowest, we get the set of eigenvectors in order of significance. The first eigenvector belongs to the largest eigenvalue and represents the most variance of the dataset. It thus points into the direction of the biggest spread in data. The second eigenvector, orthogonal to the the first eigenvector, belongs to the second largest eigenvalue and explains the second most variance.

Now every value of X_c matrix (2) can be expressed as follows:

$$x_i' = \sum_j y_j(i) \cdot e_j \tag{6}$$

with

$$y_j(i) = {X_c}^T \cdot e_j \tag{7}$$

In this new reference system, the covariance-variance reduces to the eigenvalue matrix with the n eigenvalues down the diagonal and all other elements zero.

$$\Lambda = \begin{pmatrix} \lambda_1 & 0 & \cdots & 0 \\ 0 & \lambda_2 & \cdots & 0 \\ \vdots & \vdots & \ddots & \vdots \\ 0 & 0 & \cdots & \lambda_n \end{pmatrix}$$

At this point, we can calculate how much variance is explained by each individual or a set of modes/principal components by dividing the eigenvalue of each component by the sum of eigenvalues, as shown in eq. (8).

$$EVF = \frac{\lambda_i}{\sigma_{tot}^2} \tag{8}$$

Many methods, both heuristic and statistically based, have been proposed to determine the number of important components that we should take into consideration. The most common truncation rule in PCA is the Guttman-Kaiser criterion which is the one we chose to use [12]. Principal components associated with eigenvalues derived from a covariance matrix, and that are larger in magnitude than the average of all eigenvalues, are retained.

$$\lambda_i > \frac{T}{min(m-1, n)} \sum_{j=1}^{min(m-1,n)} \lambda_j \quad \text{with } T = 1 \tag{9}$$

This criterion suits better the objectives of our study since in order to reproduce better the amplitudes of our signal, we need higher modes. Therefore, by using only the modes higher than the mean of all values we can better visualise the oscillations in the North Atlantic ocean.

Finally, for further study of the main mode of variability, the sensitivity of the first EOF coefficient to the

large-scale atmosphere variability is investigated. The climate indices used are mentioned in section 2. The climate indices are provided as monthly time series, therefore we estimated monthly correlations as well as annual ones for all of the climate indices. However, sometimes the EOF coefficient time series of the satellite data and/or the climate index are too noisy to yield useful results in a correlation analysis. In that case, the seasonal averages are calculated. The NAO, GBI, AMO, AO, TNA, AMM and FC indices are filtered using two seasonal cycles: summer (Jul-Sep) and winter (Dec-Mar). The El Niño data is filtered, by taking the average indices for the June-December months. The correlation analysis was executed in Python by using the command `np.corrcoef()` from the numpy library.

4 Results

In this section the results of our EOF analysis are presented.

The leading EOF mode of the SLA is shown in Fig. 3. It accounts for 6% of the variance over the North Atlantic sector. It has a spatial pattern of opposing sign SLA located over the Gulf Stream, with higher positive values, and over the western and northern side of the subpolar gyre, with lower negative values. Therefore, we see that the first EOF mode depicts accurately the characteristic double-gyre structure in the region. The time series of the first mode are displayed in the lower panel of Fig. 3. This plot also consists a smoothing fit through the data. Features we see are the relative maxima for the years 1995, 2001 and 2006 and an absolute minimum in the year 2011.

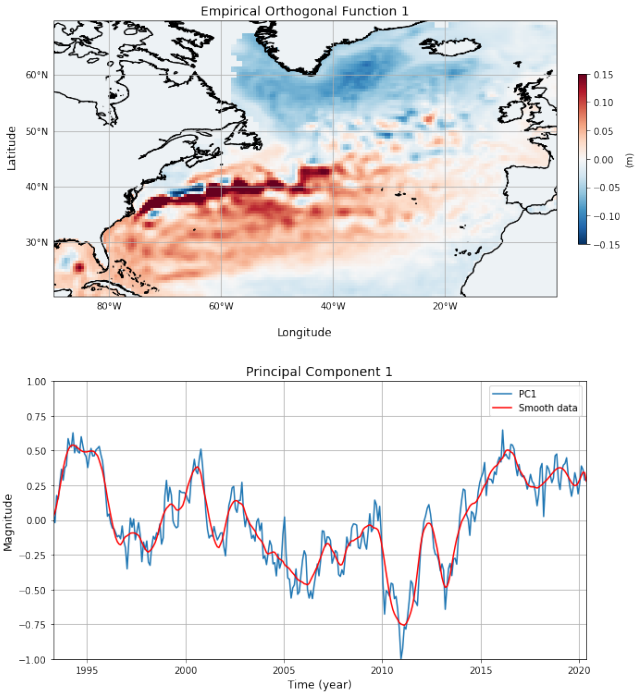

Fig. 3. The upper panel illustrates the map of the first EOF while the lower panel shows the time series of the associated EOF coefficients.

Fig. 4 shows the explained variance fraction and the cumulative explained variance fraction respectively when applying the Kaiser's rule. As we mentioned before, we see that the first mode explains around 6% of the variance and the second one explains around 3%. The first 10 components contain approximately 28.01% of the variance, while we need around 318 components to describe close to 100% of the variance. We find that the cumulative explained variance grows rapidly when including more EOF patterns. Based on Kaiser's rule, we estimate that we should use the first 86 modes, thus in Fig. 4, we only plotted these modes by notating them as red points. The variance contained in the first 86 EOFs is 77.58%.

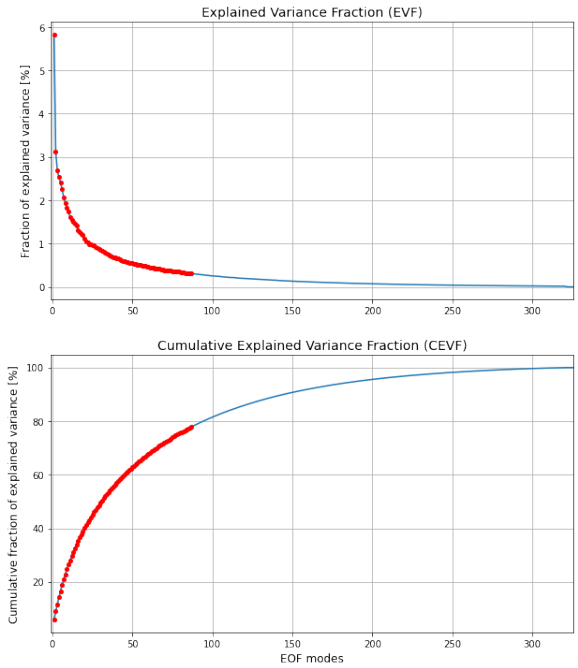

Fig. 4. The upper panel illustrates the Explained Variance Fraction (EVF) and the lower panel shows the Cumulative Explained Variance Fraction (CEVF) using the Kaiser's rule.

Fig. 5 shows the original North Atlantic SLA for the month of June 2012 and the reconstructed data with the first 86 EOFs as well as the difference between those two data values. From this figure we see that the reconstructed data is able to visualise the typical patterns occurring in our area of study.

In addition, we plot the standard deviation of the reconstructed data and its difference from the original one in Fig. 6. The comparison of the original and reconstructed plots is included in the section 5 in detail.

Finally, the time series of the climate indices that we used for the correlation analysis are illustrated in Fig. 7. No clear trend or substantial variations can be identified in the time series.

5 Discussion and Conclusions

As we can see in Fig. 3 sea level anomalies show a dipole pattern between the subpolar North Atlantic

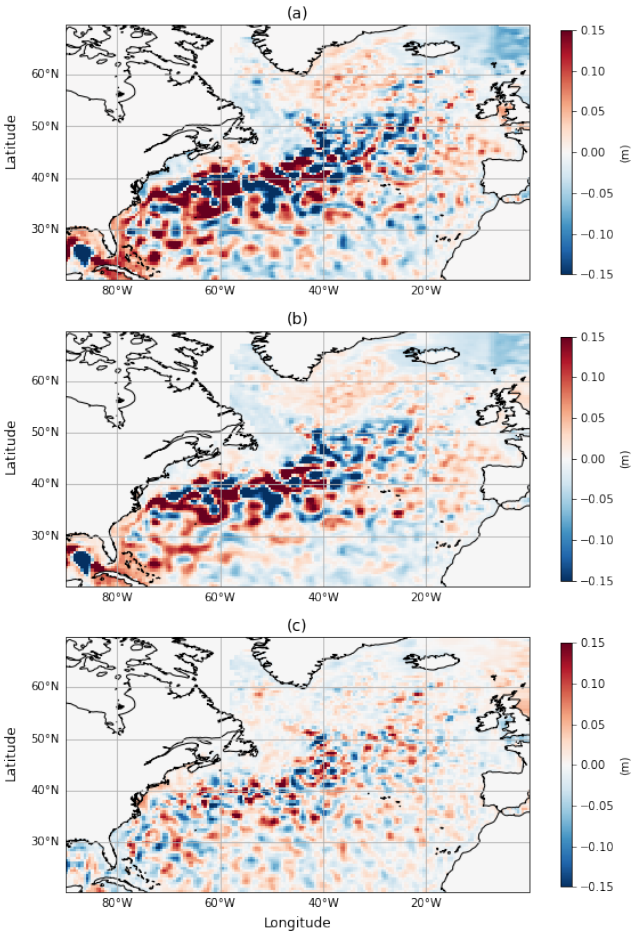

Fig. 5. North Atlantic sea level anomalies in [m] for June 2012 (a) of the original data, and (b) of the reconstructed data and (c) the difference between original and reconstructed data for the same period.

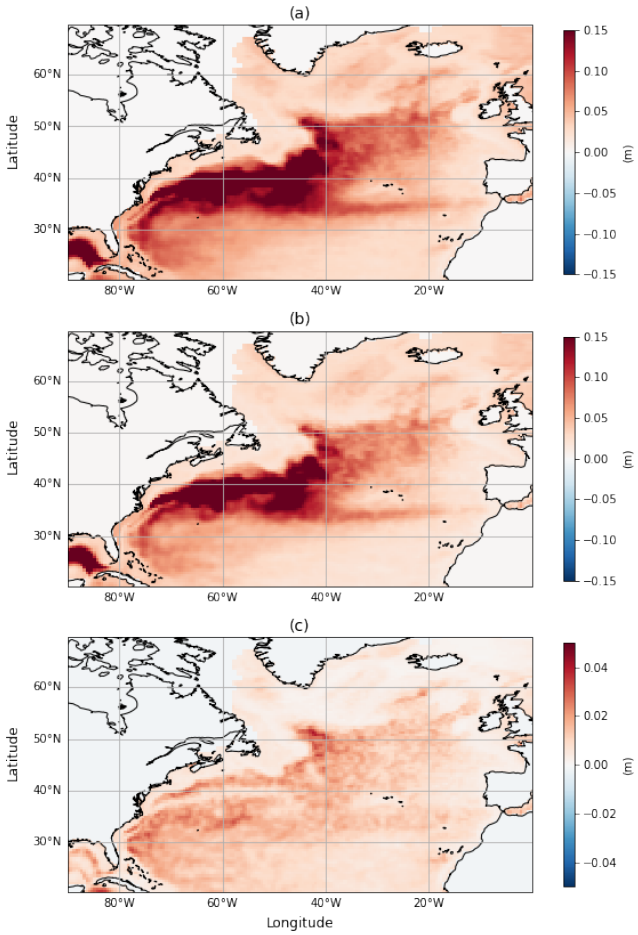

Fig. 6. Standard deviation of monthly mean sea level anomalies in [m] in North Atlantic (a) of the original data, (b) of the reconstructed data using the first 86 EOF's and (c) the difference between the original and the reconstructed data.

and the region near the Gulf Stream path. SLA in the North Atlantic is low in the cyclonic subpolar gyre and high in the anticyclonic subtropical gyre.

In Fig. 8 both the time series of the first principal component of the EOF analysis and original data are plotted to better illustrate similarities and differences. We see that the maxima of PC1 are shifted from the original data maxima with around 4 years. However the minimum is for both series around the year 2011. We cannot identify a typical time scale from neither PC1 nor the original data. Also, by looking at the fit made in the lower panel of Fig. 3 no typical timescale is recognizable. We suggest a further study using more data over a longer time span to verify if a typical timescale is present.

Since we have chosen to use the Kaisers' rule as truncation rule, we therefore reconstructed the data with the first 86 modes that explained 77.58% of the variance. Here, we will discuss the differences between the reconstructed data and the original data set.

Fig. 5 shows the North Atlantic SLA for the June 2012. When comparing (a), the original data with (b) the reconstructed data we see that the major features are visualised. As we see in Fig. 5 (c) the reconstructed data varies the most from the original data in the area of the Gulf Stream. We will see in Fig. 6 that this is the area where also the difference in standard deviation is the highest. It seems like this area is the most difficult to reconstruct as a lot of dynamics are happening here. More modes would be needed to compute a more accurate plot of the data.

The plots of the original and reconstructed standard deviation do not differ much (indeed explaining almost 78% of the variance). In Fig. 6 we plot again the standard deviation of monthly SLA for the original data as well as for the reconstructed data for the North Atlantic and their difference. In both (a) and (b) subplots we only see positive values for the standard deviation. The largest standard deviation is seen in the left, low corner where the Florida Current ends and at the location of the Gulf Stream. A minor difference can be seen when looking at how much the maximum standard deviation is spread over the North Atlantic and in Fig. 6 (c) where the difference between the reconstructed and original data is plotted. The dark red area is a bit bigger and spread out in every direction in the original plot in comparison to the reconstructed data. Indeed in the area near the Gulf Stream we see in subplot (c) the most difference. This can be explained

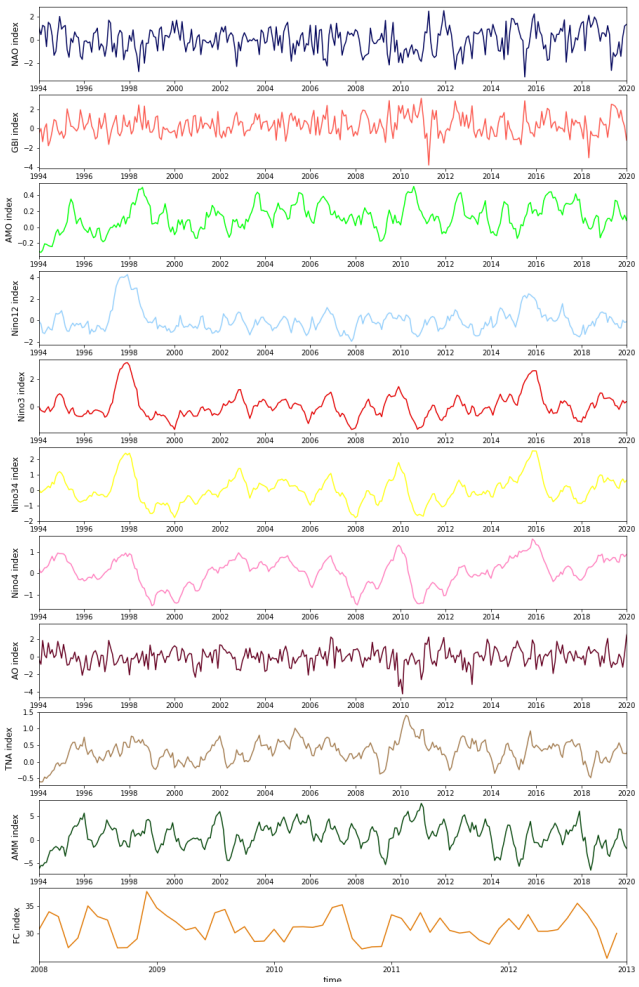

Fig. 7. Time series of the climate indices used in the correlation analysis.

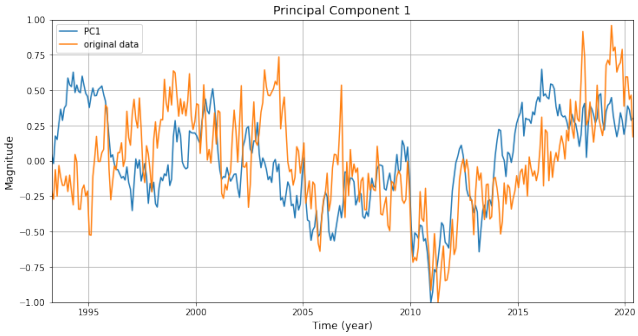

Fig. 8. Time series of the first EOF coefficient (blue line) and of the altimeter observations of sea level anomalies (orange line).

by looking at the total variance explained by the used modes. As this variance is not 100%, it is logical that the reconstructed data consists of less detailed information about the standard deviation. Nevertheless, the differences in the plot remain remarkably low with a maximum of 0.04 m at $40°W$ and $50°N$.

The results of the correlation analysis are shown in Tab. 1. The correlation coefficients vary with climate index and the time cycle, but we will focus only on the strong correlations with r $>$ 0.6. We have chosen this specific threshold in order to separate the variables that explain more than half of the variance from the others.

As we observe from Tab. 1 there is a relatively high positive correlation in winter (r = 0.71) between the first EOF coefficient and the NAO index. The NAO index corresponds to pressure differences between the Iceland Low and the Azores Islands High. When this pressure difference is higher than normal, the positive phase of NAO takes place, while when this pressure difference is lower than normal, the negative phase of NAO takes place [13]. Therefore, when low pressure systems move over a region (during the negative phase), the sea level rises, while high pressure systems push down on the ocean (during the positive phase), the sea level drops. This is called the inverse barometer effect, as the higher the pressure, the lower the sea level, and vice versa [14]. One of the possible reasons that the correlation is significant during the winter is that the variance of atmospheric forcing is strongest in the winter than in the summer. This also applies for the other climate indices as we can see in Tab. 1.

Also for the GBI index, the negative correlation is the highest for the winter period (r = -0.63). According to Bradford S. Barrett et al. (2020) [15], a positive NAO (low heights over Greenland) was related to unblocked flow, while a negative NAO (high heights over Greenland) was related to blocked flows and above-normal heights over Greenland, indicating that GBI–NAO correlations are mainly significantly negative. Since NAO is positively correlated with the sea level, GBI is negatively correlated with the sea level. The correlation is stronger during the winter because the high and low NAO values in early winter contribute to variability in the GBI while in summer contribute to an increasing trend in GBI [16].Therefore, high GBI values during winter correlate to negative sea level anomalies and vice versa.

The TNA index is a measure of the SST in the eastern tropical North Atlantic Ocean which is located just beneath the North Atlantic Ocean. From a geographical point of view this suggests correlation. From Tab. 1 we see that the annual correlation is -0.68 indicating that when TNA index is high, the SLA in the North Atlantic are low and vice versa. This suggests that the high evaporation rates caused by high SST in the Tropical North Atlantic cause SLA to be lower. If we look at the correlation in wintertime we also see this negative correlation even if with a slightly lower correlation value. The North Atlantic Circulation passes trough the Eastern Tropical North Atlantic Ocean and is negatively effected by the SST as we see from the correlation Tab. 1.

The AMM is a measurement of variability caused by both the ocean and atmosphere. The AMM consist of variations in meridional SST gradients near the intertropical convergence zone (ITCZ), surface wind anomalies, a shift of the ITCZ toward the anomalously warmer hemisphere and enhancement of the trades over anomalously cold water resulting in evaporation

which reinforces cold and warm weather. This has significant effects on the SLA in the north Atlantic ocean. We see from Tab.1 negative correlation (r = -0.76) between the two variables [6]. The positive AMM describes weak trade winds which are associated with less mixing and upwelling [17], resulting in warmer northern tropical Atlantic SST anomalies, and vice versa during the negative AMM [18]. As we mentioned above, the high evaporation rates caused by high SST in the Tropical North Atlantic cause SLA to be lower.

Moreover, since the Florida Current is located in the lower left part of our area of study and currents can have effect on the sea level height, we wanted to also take into account the correlation between the North Atlantic Ocean SLA and the Florida Current. Indeed we see high positive correlation (r = 0.88) indicating the same behaviour between the SLA in the North Atlantic Ocean as those in the Florida Current. According to Park et al. (2015) [19], Florida Current transport is dynamically linked to coastal sea level anomalies through geostrophic balance between the sea level and mass transport.

Finally, for the AO, AMO and the different NINO indices, we do not find any high correlations. Since the correlation between the EOF and the AMM is strong, the correlation between our data and El nino indices is weak. Also, since our data set does not contain the long-term trend, seasonality is removed and the dataset is short in length compared to the multidecadal timescale of the AMO, the respective correlation is low.

Our study is computed over data with a large time span of 27 years and a large regional space covering the North Atlantic Ocean. Therefore, it can be difficult to analyse the interannual oscillations and its correlations as signals can cancel each other out in the time span of months/years or space. This can be seen as a limitation for this study when trying to find correlations. Results could be improved by looking at shorter time intervals for instance comparing one month over 27 years. We already tried to analyse the seasons and this improved our results especially when looking at the winter period. Another way to improve our results is by looking at separate regional domains of the North Atlantic. For example, it would be interesting to investigate the interannual variations of the 'North' region where the supbolar gyre exists and the 'South' region where the suptropical gyre exists, separately. This could highlight the different underlying mechanisms that determine how oceanic signals respond to external forcings at each different domain. Overall, this study indicates the potential of using the altimeter observations to examine the interannual variability of the North Atlantic Ocean Circulation and the sensitivity of these variations to the large-scale atmosphere variability. Future work is needed to investigate with more details the North Atlantic Ocean Circulation.

Climate index	Correlation coefficient				
	Monthly	Annually	Summer	Winter	Jul-Dec
NAO	0.24	0.48	0.11	**0.71**	
GBI	-0.19	-0.29	-0.15	**-0.63**	
AMO	-0.28	-0.34	-0.35	-0.27	
AO	0.19	0.32	0.26	0.50	
TNA	-0.52	**-0.68**	-0.55	**-0.60**	
AMM	-0.53	**-0.76**	-0.53	**-0.73**	
FC	0.17	**0.88**	0.22	0.49	
NINO12	0.12	0.12			0.17
NINO3	0.18	0.22			0.21
NINO34	0.25	0.31			0.28
NINO4	0.32	0.36			0.38

Tab. 1. Correlation values between PC1 and different climate indices over various time intervals

References

Wikipedia contributors. Atlantic ocean — Wikipedia, the free encyclopedia. URL: https://en.wikipedia.org/wiki/Atlantic_Ocean, 2021. [Online; accessed 25-October-2021].

Alan Buis. Sea level 101: What determines the level of the sea? Ask NASA Climate, blog. URL: https://climate.nasa.gov/blog/2990/sea-level-101-what-determines-the-level-of-the-sea/, 2020. [Online; accessed 27-October-2021].

European Organisation for the Exploitation of Meteorological Satellites (EUMETSAT). The altimetry technique. URL: https://www.eumetsat.int/altimetry-technique. [Online; accessed 23-October-2021].

Xiaoli Deng. *Satellite Altimetry*, pages 1–5. Springer International Publishing, Cham, 2016.

Bert Wouters. Hand-in 2: Remote-Sensing, 2021.

Dan Vimont. The Atlantic Meridional Mode. URL: https://www.aos.wisc.edu/~dvimont/MModes/AMM.html, 2015. [Online; accessed 27-October-2021].

Physical Sciences Laboratory. Monthly Climate Timeseries: Atlantic Meridional Mode (AMM) SST Index. URL: https://psl.noaa.gov/data/timeseries/monthly/AMM/, 2021. [Online; accessed 27-October-2021].

Zakaria Jaadi. A step-by-step explanation of principal component analysis (pca). URL: https://builtin.com/data-science/step-step-explanation-principal-component-analysis, 2021.

Bert Wouters. Lecture 6 - Remote Sensing - part2. *Utrecht University, Institute for marine and atmospheric research*, 2021.

Wikipedia contributors. Eigenvalues and eigenvectors — Wikipedia, the free encyclopedia. URL: https://en.wikipedia.org/w/index.php?title=Eigenvalues_and_eigenvectors&oldid=1050942733, 2021. [Online; accessed 23-October-2021].

Steven Holland. LECTURE NOTES - Principal Components Analysis. URL: http://strata.uga.edu/8370/lecturenotes/principalComponents.html, 2021. [Online; accessed 23-October-2021].

J. E. Jackson. *A user's guide to principal components*. John Wiley Sons, 2005.

Rebecca Lindsey and Luann Dahlman. Climate Variability: North Atlantic Oscillation. NOAA Climate.gov. URL: https://www.climate.gov/news-features/

understanding-climate/climate-variability-north-atlantic-oscillation, 2021. [Online; accessed 27-October-2021].

Craig Brokensha. The Inverse Barometer Effect. Swellnet, blog. URL: https://www.swellnet.com/news/swellnet-analysis/2016/04/19/inverse-barometer-effect, 2016. [Online; accessed 27-October-2021].

Bradford S Barrett, Gina R Henderson, Erin McDonnell, Major Henry, and Thomas Mote. Extreme greenland blocking and high-latitude moisture transport. *Atmospheric Science Letters*, 21(11):e1002, 2020.

Edward Hanna, Xavier Fettweis, S. Mernild, John Cappelen, Mads Ribergaard, Christopher Shuman, Konrad Steffen, Len Wood, and Thomas Mote. Atmospheric and oceanic climate forcing of the exceptional greenland ice sheet surface melt in summer 2012. *International Journal of Climatology*, 34, 03 2014.

Enrico Scoccimarro, Alessio Bellucci, Andrea Storto, Silvio Gualdi, Simona Masina, and Antonio Navarra. Remote subsurface ocean temperature as a predictor of atlantic hurricane activity. *Proceedings of the National Academy of Sciences*, 115(45):11460–11464, 2018.

Christina M Patricola, R Saravanan, and Ping Chang. A teleconnection between atlantic sea surface temperature and eastern and central north pacific tropical cyclones. *Geophysical Research Letters*, 44(2):1167–1174, 2017.

J Park and W Sweet. Accelerated sea level rise and florida current transport. *Ocean Science*, 11(4):607–615, 2015.